Image-guided thermal ablation with MR-based thermometry

Mingming Zhu, Ziqi Sun, Chin K. Ng

Department of Radiology, School of Medicine, University of Louisville, Louisville, KY, USA

Correspondence to: Chin K. Ng. ULH, Radiology, CCB-C07, 530 S Jackson Street, Louisville, KY 40202, USA. Email: chin.ng@louisville.edu.

Abstract: Thermal ablation techniques such as radiofrequency, microwave, high intensity focused ultrasound (HIFU) and laser have been used as minimally invasive strategies for the treatment of variety of cancers. MR thermometry methods are readily available for monitoring thermal distribution and deposition in real time, leading to decrease of incidents of normal tissue damage around targeted lesion. HIFU and laser-induced thermal therapy (LITT) are the two widely accepted tumor ablation techniques because of their compatibility with MR systems. MRI provides multiple temperature dependent parameters for thermal imaging, such as signal intensity, T1, T2, diffusion coefficient, magnetization transfer, proton resonance frequency shift (PRFS, including phase imaging and spectroscopy) as well as frequency shift of temperature sensitive contrast agents. Absolute temperature mapping techniques, including both spectroscopic imaging using metabolites as a reference and phase imaging using fat as a reference, are immune to susceptibility effects and are not dependent on phase differences. These techniques are intrinsically more reliable than relative temperature measurement by phase mapping methods. If the limitation of low temporal and spatial resolution could be overcome, these methods may be preferred for MR-guided thermal ablation systems. As of today, the most popular MR thermal imaging method applied in tumor thermal ablation surgery is, however, still PRFS based phase mapping technique, which only provides relative temperature change and is prone to motion artifacts.

Keywords: MR thermometry; tumor thermal ablation; thermal dosimetry; high intensity focused ultrasound (HIFU); laser induced thermal therapy (LITT); MR guided thermal ablation

Introduction

Heat-based tumor ablation techniques using thermal energy sources such as radiofrequency, microwave, high intensity focused ultrasound (HIFU) and laser have received much attention as minimally invasive strategies for the treatment of malignant and benign tumors in a variety of organs. Potential benefits of these therapies include the ability to treat tumors focally on non-surgical patients, potential to perform on an outpatient basis and reduced morbidity as compared to surgery. For decades, these methods were applied with limited knowledge of thermal distribution and deposition in the target area, but rather relied greatly on the experience of the surgeon who performed the ablation surgery. With a rapid development of image guided thermal therapy techniques in recent years, especially magnetic resonance imaging (MRI) guided thermal interventional surgery techniques, heat-based tumor ablation has demonstrated its clinical potential and becomes widely accepted as a replacement of traditional surgical ablation. The benefit of using MRI on tumor thermal ablation are two folds: (I) MRI provides unsurpassed soft tissue contrast and detailed three dimensional view at the lesion area for an accurate heat source positioning, lesion targeting and tissue damage monitoring during surgery, immediately after, and long term follow-up; (II) a variety of MR thermometry methods are readily available for monitoring thermal distribution in real time, thus effectively guides the thermal deposition and decreases incidents of normal tissue damage around targeted lesion.

Conventional temperature monitoring techniques *in vivo*, such as fiber optics and thermocouples, are fast in response and accurate in temperature measurements. However, these techniques are invasive and localized, and produce low spatial resolution (1-4). To overcome these limitations, MR thermometry has been developed to non-invasively measures tissue temperature in a 3D volume with high spatial and temporal resolution (5-8). In addition, MR thermometry opens up the opportunities of performing multi-functional imaging and MR temperature imaging (MRTI) guided hyperthermia treatments (6,9). The first MR thermometry developed was based on temperature dependence of T_1 relaxation time constant of water molecules (10). Soon after that, MRTI of tissue water molecules using diffusion coefficients (11), proton spin density (12), proton resonance frequency shift (PRFS) (13,14), proton chemical shift (15,16), magnetization transfer (17), and temperature sensitive contrast agents (18), have been developed. Among these MRTI methods, PRFS methods demonstrate the highest sensitivity to temperature changes over a broad temperature range and is commonly used in regional hyperthermia therapy (19). The accuracy of the temperature measurements using MR thermometry is comparable to that of the invasive methods (20). However, conventional MR thermometry methods, such as PRFS, are sensitive to local magnetic susceptibility associated with tissue anatomy and interventional medical devices (21-23), large fat contents within the region of interest (ROI) (14), motion artifacts (5), and magnetic field drift (20). Alternative MR thermometry techniques have been developed over the last twenty years to exploit MR properties that afford high temperature sensitivity and measurement accuracy. In addition, MR thermometry techniques also provide a means to measure absolute tissue temperature, which is essential in some of MRTI applications. One approach is to use the spectroscopic imaging technique to obtain absolute temperature values by using tissue lipid or brain metabolites such as N-Acetyl Aspartate as the internal reference (15). In recent development, MR thermometry using water-fat chemical shift difference has been used to remove temperature measurement errors caused by local field inhomogeneity (24,25). With these technical improvements, MR thermometry has found wide applications in medicine, particularly in the areas of MRI guided regional hyperthermia treatments (19,26-28).

In this review, the needs for accurate temperature monitoring in clinical tumor thermal ablation are discussed. Several emerging thermal ablation applications are presented. Furthermore, technical aspects of each commonly used MR thermometry methods are reviewed. The strength and limitations of these methods are also discussed.

Overview of imaging-guided tumor thermal ablation

There are two categories of thermal therapy depending on the treatment scheme. The first type of tumor hyperthermia is induced and controlled at ~43–45 ℃ for tens of minutes in order to kill tumor cells or enhance the effect of radiation therapy (29). The second type is to quickly induce higher temperature (50–80 ℃) and maintain at a shorter period (normally in the order of several seconds) to rapidly coagulate the tissue and ensure tumor tissue necrosis (30). The latter is referred to as tumor thermal ablation and is more broadly used. Recent development of medical heat induction techniques such as interstitial laser therapy (ILT), radiofrequency therapy (RF), microwave and high-intensity focused ultrasound therapy (HIFU) have expedited the clinical use of minimally invasive thermal ablation techniques on cancer patients (*Table 1*). However, despite the advancement of the tumor ablation techniques, the initial efforts suffered greatly from the lack of monitoring temperature reliably to guide the surgery and to prevent collateral damage to normal tissue surrounding the tumor. With the introduction of MRI as a tool to simultaneously provide anatomical details of tumor location and monitor temperature distribution and heat deposition in the targeted tissue, the combined technique has drawn great attention in the field of tumor thermal ablation during recent years. It is worth to point out that, although cryoablation is an important aspect of tumor ablation technique due to its unique tissue killing mechanism comparing to other thermal ablation techniques mentioned above, it is not applicable in the following discussion about thermal dosimetry.

Current MR-guided tumor ablation techniques

One of the most commonly used thermal ablation technique is called radio frequency ablation (RFA), which makes use of high frequency alternating RF current to generate heat. Variable dimensions of the RF probes have been made to accommodate diverse tumors in various organs. RFA procedures can be performed under image guidance, such as CT (32) and ultrasound (33), but not MRI due to

Table 1 Comparison of various ablation techniques (31)

Type of ablation	Mechanism	Advantages	Disadvantages
Cryoablation	Killing tumor tissue by cooling and reheating (Freeze-thaw cycle)	Less pain; can create large lesion and is effective in multiple lobes of tumors	Significantly affected by blood flow; high complication rate
Ultrasound	Heating generated by focusing low energy ultrasound beams from multiple sources	Compatible with MRI. Ability to focus the area of treatment without direct contact. Good depth of penetration. Fast development of image-guided high intensity focused ultrasound (HIFU) applications	Requires general anesthetic. Not small enough for use in catheters. Ablation time is long. Cannot be directed through air-filled viscera such as the lung
Radiofrequency	Resistive heating by alternating radiofrequency electrical current	Widely available. Simple design and proven effectiveness. Ability to treat different tumor types	Direct contact with object required. Incomplete ablation near blood vessels due to heat removal by blood flow
Microwaves	Heating by propagating electromagnetic waves	High temperature available. Capable of forming large lesions in the presence of blood perfusion	Complications include pleural effusion, hemorrhage, and abscess
Laser	Laser light induced heating using different wavelengths	Fully compatible with MRI. Can deliver controlled low energy through various fiber configurations to achieve thin, continuous lesions	Expensive equipment. Small ablation zone. Tissue charring around the tip of the fiber

its interference with MRI detector. Microwave ablation is another technique that uses tissue heating to replace surgical removal of tumor. By using electromagnetic waves in the 300 MHz to 300 GHz range in the microwave energy spectrum, specially made microwave antennas are positioned near or inside the targeted tumor tissue. Comparing to RFA, microwave ablation is reported to have larger and more circular ablation zone, better defined ablation edge (34), and the advantage of having multiple applicators simultaneously for larger tumors (35).

Among all the emerging MR-guided thermal ablation techniques, HIFU and laser-induced thermal therapy (LITT) have gained widespread acceptance in interventional tumor thermal ablation procedures due to their compatibility with MRI. This is because, unlike other thermal ablation heat sources, focused ultrasound is a noninvasive therapy which does not require contact with the targeted focal area. This is especially beneficial to be used together with MRI, which leads to artifact-free anatomical and thermal imaging. Although requires contact with the targeted lesion, laser induced thermal therapy commonly uses fiber-optic probe, which does not produce large image artifacts caused by electromagnetic interference, as in RFA. The feasibility of performing MR guided high intensity focused ultrasound (MRgHIFU) and MR guided laser-induced thermal therapy (MRgLITT) has been established and further demonstrated by treating tumors in brain (27,36-39), prostate (40,41), and liver (30,42,43).

MRgHIFU

With over half a century of development since the first clinical use of HIFU ablation on cancer treatment (44,45), this technique has become a relatively mature alternative to traditional invasive tumor ablation techniques. HIFU allows for noninvasive focal delivery of energy into several millimeters of soft tissues beyond the surface (modifying and eliminating tissue for therapeutic purposes. However tumor targeting and heat monitoring were among the several issues in the original design of HIFU ablation technique until the combined use of non-invasive temperature and anatomical guidance with MRI. The fast development of MRgHIFU in the last decade has enabled the wide acceptance of the technique in clinical treatment of malignant and benign tumors to the extent that it has become a routine operation in some hospitals (30,46).

The first clinical feasibility study of MRgHIFU study was reported by Hynynen *et al.* on benign breast fibroadenomas patients (47). A clinical MRI compatible ultrasound surgery system (GE Medical Systems) was used with a half-intensity ultrasound beam diameter and length of 1.0 and 4.8 mm respectively. The MR imaging was performed not only during each tumor ablation to localize heat distribution, but also after treatment in order to verify tissue viability and monitor long term effect. The strategy to ablate the whole tumor tissue was to heat a small region of tissue sequentially with an acoustic power of 28–50 W for 10 s in 50 s intervals.
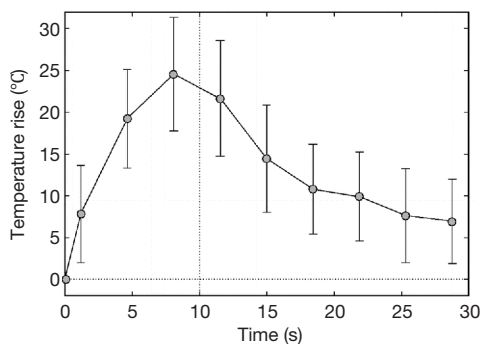
　　　　qims.amegroups.com 　　　　*Quant Imaging Med Surg* 2017;7(3):356-368

Figure 1 Graph shows mean temperature elevation as a function of time of the hottest voxel, as measured by MR imaging-derived thermometry. The temperature increase was 17.5–45.2 ℃. Heating exposure time was 10 s. A total of 71 sonications in three planes were delivered to a breast fibroadenoma (47).

The individual ablations were closely packed with an average focal distance of 2.8 mm. The author estimated the time needed for the treatment of a 2-cm lesion was about 2 hours. The choice of reducing the heat exposure time to 10 s is to minimize the effect of local blood perfusion, which may confound heat buildup in each application of acoustic ablation and prevent obtaining a homogenous coagulation of tumor tissue (see *Figure 1*). Such a strategy is widely accepted and further improved with a more complicated spatial pattern such as continuous sonication with spiral trajectory of the focal point (48-50). In a similar approach, MRgHIFU is also applied on treatment of uterine fibroids. The first and only FDA-approved MR guided ultrasound device to treat uterine fibroids is the Exablate 2000 system (InSightec, Haifa, Israel), which was introduced in 2004. The technique is to reduce the fibroids mass volume by thermal ablation and to induce large nonperfused areas with the aim of fibroids shrinkage (51,52).

MRgLITT

LITT, or sometimes referred as ILT is a procedure for destroying tumor tissue using heat generated by laser light absorption at certain wavelength. The laser radiation is delivered directly to the target tissue via an optical fiber. The distal fiber end is usually equipped with a specially designed tip, which is positioned in the center of the tumor area. Due to high temperature induced by laser light, the technique normally involves placing a water or saline-cooled catheter into the lesion area so that both the tip of the fiber-optic cable and heating region of the tissue can be continuously flushed to prevent overheating. Comparing to other thermal ablation techniques, LITT may exhibit a more precise energy deposition and thus a better-defined boundary of the thermal ablation zone due to the smaller heating tip. In addition, LITT is highly compatible with MRI. Functioning similarly as in MRgHIFU, MR anatomical imaging and thermal imaging in MRgLITT can be used to aid tumor localization, probe positioning, monitoring of the thermal ablation zone, as well as post-treatment verification of tumor coagulation area and follow-up. LITT was investigated for treatment of cerebral neoplasms as early as the 90s (53), but real-time imaging was not performed at that time. Subsequently, LITT has been applied on brain tumor patients with simultaneous T1-weighted MRI, which allowed qualitative but not quantitative visualization of laser heating (54,55), and has been investigated for palliative treatment of high-grade gliomas (37). More recently, proton resonance shift (PRS) based MR thermal imaging has been applied in MRgLITT and further used for treatment of primary brain tumors (36,38,56). These clinical trials have focused on metastatic tumors of extracerebral origin because such tumors are excellent candidates for complete ablation by a single intracranial laser treatment. Currently, there are two FDA-approved commercially available LITT thermal ablation systems in the market. The first one is Visualase Thermal Therapy System (Visualase, Inc., Houston, TX, acquired by Medtronic in 2014) which uses 15W, 980-nm diode laser and combined with water cooled laser applicator system. The other one is the NeuroBlate System, formerly known as the AutoLITT System (Monteris Medical, Inc., Plymouth, MN) which uses 1,064-nm wavelength (e.g., Nd:YAG or tuned diode laser) combined with CO_2 cooling. A phase I trial on the feasibility of using Visualase MR-guided LITT device on low-risk prostate cancer has been reported (*Figure 2*) (57). Recently, MRI-guided laser interstitial thermal therapy for the treatment of low-grade gliomas in children using both systems have been reviewed (58).

Challenges in MRI guided thermal ablation

As previous mentioned, thermal ablation benefits from imaging guidance not only because it provides detailed anatomical information before and after surgery, but also the accurate temperature monitoring and thus possible on-the-fly thermal dose calculation and regulation.

Even though there are different methods used for temperature mapping by MRI (6,7,59), almost all clinical
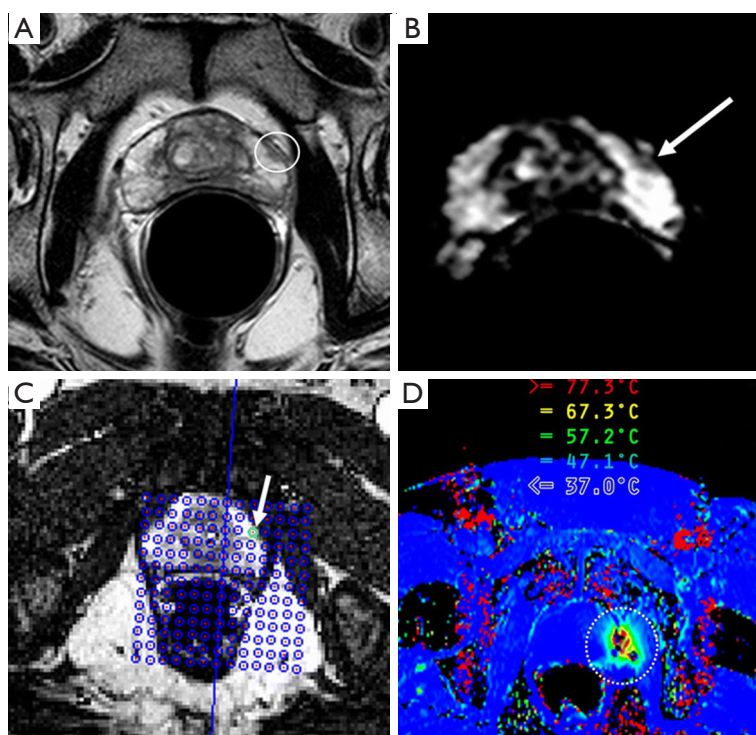
Figure 2 MR Images of a 55-year-old man with biopsy-proved prostate cancer with Gleason score of 6 in a single core from left lateral base of peripheral zone of prostate (57). (A) T2-weighted axial fast spin-echo image through prostate base shows focal hypointense area within left peripheral zone anterior, which is indicative of cancer. (B) Apparent diffusion coefficient map through same level shows a concordant focal area of low signal intensity (arrow). (C) MR image demonstrates how prostate cancer is targeted with transperineal grid and software. Green circle (arrow) indicates appropriate hole for insertion of trochar. After a test dose of laser energy, which was sufficient to cause detectable thermal change but insufficient to cause injury, an axial image plane was used to visualize thermal changes and damage estimates during treatment. (D) MR thermography image shows increased temperature in target areas (circled), which are updated every 3–5 s. Black pixels in heated region likely indicate artifacts.

and research studies currently use temperature dependent PRFS (13,22,60) as a measure of temperature elevation, due to its simplicity as well as relatively high spatial and temporal resolution. With fast development of MR thermometry methods, many novel and advanced sequences have been developed in recent years. Some of them have claimed to have overcome issues like motion and susceptibility artifacts. Thus, it is timely to review these methods and assess the pros and cons of the different strategy of MR thermometry as we are seeking for the next preferred method for MRI guided thermal ablation.

In the following discussion, we'll start with the importance of controlling the temperature in heat-based tumor cell killing (tumor thermal dosimetry) and then go over a gallery of currently available MR thermometry methods. Advantages and disadvantages of each method will

also be discussed in the end.

Tumor thermal dosimetry

The control of the heat deposition is an important aspect of thermal treatment of tumors. With the convenience of obtaining tissue temperature non-invasively using MRI, real time thermal dose can be monitored and regulated. The relationship between temperature (T) and cell death rate has been empirically derived from cell culture experiment and approved to also apply for *in vivo* systems (61). *Figure 3* depicts cell survival response to heat for human cells as well as comparing to both pig and mouse. These studies show that the rate of cell killing during exposure to heat is exponential and dependent on the temperature as well as the time during the exposure. The relationship of heat induced
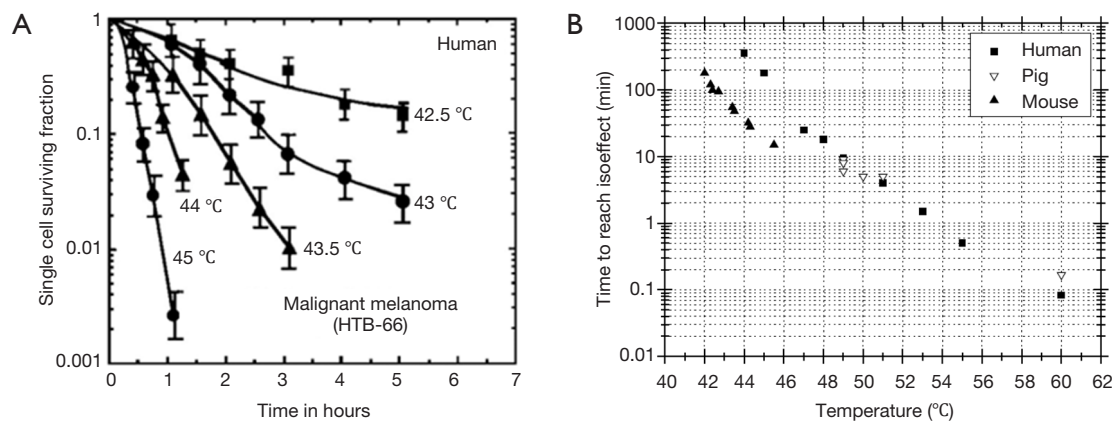
Figure 3 The response of human and animal cells to temperature. (A) Survival of a human melanoma cells, heated over a temperature range of 42–45 ℃. (B) Time to reach epidermal necrosis as a function of temperature for mouse, human and pig skin over a temperature range of 42–60 ℃. Note that the thermal sensitivities of pig and human skin are virtually identical and both appear to be more resistant to thermal damage than mouse skin (62).

cell inactivation rate and temperature can be described by Arrhenius Equation and can be expressed as following:

$$k = e^{-E_a/R_g T} \qquad [1]$$

where k is the *rate* of heat induced cell death, E_a is the activation energy, and R_g is the universal gas constant. The relationship has led to several different methods for normalizing time-temperature data to a common unit that would allow for comparison of different heating regimes. Sapareto and Dewey (61) proposed a simple method called "thermal isoeffective dose" for this purpose.. It describes heat exposure time (t) and temperature (T) correlation for two equivalent thermal doses during treatment of tumor:

$$t_1 = t_2 R^{(T_1 - T_2)} \qquad [2]$$

where constant R can be either 0.5 (when T ≥43 ℃) or 0.25 (when T <43 ℃). The equation describes that applying heat to maintain a tissue temperature of 43 ℃ for 240 min has equivalent treatment effect as heating the tissue at 60 ℃ for 0.1 s. This is particularly important for clinical applications of thermal ablation, since temperatures during heating are typically spatially non-homogenous and varies temporally during heating and cooling. Thus, with adequate spatial and temporal resolution, a well-designed MRI temperature mapping technique can be used to adjust the power of heat source so that the thermal dose can be carefully controlled. With the help of online thermal data analysis and simultaneous dose calculation, a close-loop thermal ablation system can be designed for automated dose control during

tumor thermal ablation (14).

One must also pay close attention to the maximum temperature allowed for heating targeted tumor tissue. With tissue heating close to or above 100 ℃, water boiling may occur, thus unwanted air bubble can be generated to complicate the tumor thermal treatment (59). For example, uncontrolled heat conduction change due to air bubble in targeted area may induce an over-estimation of thermal dosage in the area, leading to an incomplete thermal ablation. At the same time, disturbance in the local susceptibility at air-tissue interface may have severe effect on local phase, thus invalidate the PRFS based MR thermometry methods around the bubble area.

MR thermometry methods

In vivo MR thermometry methods can be classified into two categories. One is to measure the temperature change relative to a reference temperature. In the regional hyperthermia treatment, a reference temperature image is acquired before the interventional treatment is applied to the ROI. Thus tissue temperature changes induced by MR parameter changes are extracted from the MR images collected before and during treatment. Another category involves monitoring tissue temperatures in absolute scales using internal reference signals, such as lipid signal which is independent of temperature change. In the following section, both categories of MR thermometry methods and the related applications are discussed.

　　　qims.amegroups.com　　　*Quant Imaging Med Surg* 2017;7(3):356-368

Table 2 Summary of MR-based techniques for measuring relative temperature

Method	Principle	Advantages	Disadvantages	References
T_1 relaxation time constant	As temperature increases, the motion rate increases, resulting in a greater exchange rate between water molecules. Relative temperature is measured using: $\Delta T = c\Delta T_1$	Readily available imaging sequences	Low temperature sensitivity (1%/℃); other factors can change T_1; the apparent T_1 relaxation time constant is the weighted average of T_1s of water molecules in tissue microstructures. This could cause a nonlinear dependence of T_1 on temperature	(63)
T_2 relaxation time constant	A linear relationship between T_2 and temperature (T) exists for the free water model	Can be used for adipose tissues; higher sensitivity than T_1 (10%/℃)	More difficult to measure than T_1 due to shorter T_2 values; irreversible T_2w signal change at high tissue temperature due to tissue damage.	(17,63,64)
Diffusion coefficient (D)	The diffusion coefficient (D) is linearly related to the temperature through a Strokes-Einstein equation	Readily available imaging sequences	Low temperature sensitivity (2%/℃); other factors can change diffusion coefficient (D)	(19,65)
Proton density (PD)	Water proton density is inversely proportional to the tissue temperature	Independent of tissue type; readily available imaging sequences	Very low temperature sensitivity (0.29%/℃)	(66)
Magnetization transfer (MT)	The signal intensity, magnetization transfer ratio ((M0-MT)/M0) correlates non-linearly with tissue temperature	Can be used together with other MT applications	Quantitative relationship between MT signal intensity and the chemical exchange rate as a function of temperature has not been reported; non-linear function of tissue temperature; Tissue-type dependent.	(67-69)
Proton resonance frequency shift (PRFS)	Water hydrogen bond disruption at elevated temperature results in increased shielding constant, and thus decreased chemical shift (frequency) for water protons	Fast temperature mapping techniques readily available; linear function of tissue temperature; independent of tissue type (non-fat tissue)	Cannot be applied for fat tissue; relatively low temperature sensitivity (0.01 ppm/℃)	(13,22,60)

Relative temperature measurements

Water proton density, T1, T2, diffusion coefficient, magnetization transfer, and PRFS are correlated with temperature changes, and all can be used for relative temperature measurement. These methods have been extensively studied and thoroughly reviewed in other publications. *Table 2* summarized all the MR based relative temperature measurement methods as well as their advantages and disadvantages.

Absolute temperature measurements

Currently PRFS method is the most widely used thermometry method in the clinic because it has high temporal and spatial resolutions, is insensitive to tumor tissue type (non-fatty tissue) and can be integrated with MR compatible heating devices. However, the PRFS method measures only relative temperature changes instead of absolute temperature.

Although generally more complicated and time consuming, there are other MR based thermometry methods that can be used for absolute temperature quantification.

Proton frequency referenced by lipid or NAA in magnetic resonance spectroscopy (MRS)

In many cases, measuring absolute temperature is more desirable than measuring relative temperature change. Several MRS based methods have been developed to directly measure absolute temperature. These methods are different from the basic PRFS by the fact that an internal reference is used to eliminate possible field related artifacts. Fat (15,70) and brain metabolite (16,24,71-73) peaks are often chosen as the temperature independent references, depending on the ROI (around tumor tissue or inside the brain). The feasibility of the MRS based MR thermometry method has been validated in several early publications over

two decades ago when the technique was first invented to help neuroscientists to quantify brain temperature (71,72). The advantages of the technique are three folds. Firstly, since both water and metabolites experience the same field within each voxel (for example, in single voxel MR spectroscopy), the phase shift due to inhomogeneities cause by shimming and B0 field drift during scan can be largely eliminated through deduction of reference frequency from the water peak. Secondly, the correlation of frequency difference of water (or metabolites) and temperature has been found to be independent of tissue types, protein content ratio, or pH in physiological range. Thirdly, metabolites are widely distributed in the targeted tissue (N-Acetylaspartate, NAA in brain or lipid in tumor tissue). The correlation of temperature and water – NAA (or lipid) frequency difference does not depend on pH in the range of 5.5 to 7.6 (74). In addition, change of this correlation is insignificant when protein level is between 80 and 100 mg/mL (72). This MR thermometry method largely eliminates field drift or non-uniform field distribution by using the internal reference. Magnetic resonance spectroscopic imaging (MRSI), or sometimes referred to as chemical shift imaging (CSI) of temperature mapping has been further developed after the success of the single voxel MRS absolute temperature quantification technique (15,16,24,75).

Although these MR spectroscopy methods have demonstrated promising potential for accurate mapping of absolute temperature in biological systems, they unfortunately still have many disadvantages preventing their use in real time temperature monitoring: (I) relatively long acquisition time (typically on the order of a couple of minutes), thus low temporal resolution and poor spatial resolution comparing to other thermal imaging methods; (II) highly dependent on a homogeneous magnetic field to obtain accurate frequency measurement; (III) rely on accurate measurement of low concentration metabolites, thus, not applicable under some pathological conditions (e.g., tumor necrosis). Some of these limitations have been mitigated by new imaging strategies such as fast MRSI methods using echo-planar spectroscopic imaging (15). However, further development of the method is needed to reach clinical implementation of the technique.

Temperature mapping using water-fat proton chemical shift difference

Besides spectroscopy methods, absolute temperature

mapping techniques using imaging approach were also developed. For internal reference, such as the fat proton frequency, the water proton chemical shift as a function of temperature is as follows (16):

$$\delta_{wf}(T) = -\Delta\sigma_{wf}(T) \times 10^6 \qquad [3]$$

where δ_{wf} is the water proton chemical shift in ppm referenced to that of the fat protons, $\Delta\sigma_{wf}$ is the shielding constant difference between water and fat protons, whereas the temperature dependence of $\Delta\sigma_{wf}$ comes from the water protons. For external reference using water proton resonance frequency at a reference temperature, the chemical shift of water protons at specific temperature is a function of shielding constant and volume magnetic susceptibility at that temperature (16). That is,

$$\delta_w(T) = \left[-\Delta\sigma_w(T) + s\Delta\chi(T)\right] \times 10^6 \qquad [4]$$

where δ_w is the chemical shift of water protons in ppm, Δ_w is the shielding constant change relative to that of the reference temperature, s is a factor related to the shape of the object, and $\Delta\chi$ is the volume susceptibility change relative to that of the reference temperature.

A chemical shift selective phase mapping method was developed to enhance the temporal resolution (25). In this method, two sets of images were collected at each temperature point using a 2D gradient echo sequence. In one set of images, water signal was selectively suppressed while the fat signal was acquired. In another set of images, the reverse order was performed. The phase difference between the water and fat signals can be calculated from the complex signals of the two sets of images, and is related to the temperature sensitivity through the chemical shift difference between fat and water protons as follows:

$$\varphi_{wf} = \arg\left(s_w s_f^*\right)$$

$$= \tan^{-1}\left[\frac{Re(s_f) \times IM(s_w) + Re(s_w) \times IM(s_f)}{Re(s_w) \times Re(s_f) + IM(s_w) \times IM(s_f)}\right] \qquad [5]$$

$$= \text{mod}\left(\delta_{wf} \times w_{RF} \times TE, 2\pi\right)$$

where S_w and S_f are complex signals of water and fat protons with the corresponding real and imaginary parts of Re[ ], and Im[ ], respectively, ω_{RF} is the angular RF frequency, and TE is the echo time. This method has about the same temperature coefficient (0.01 ppm/°C) as that of the CSI method but much higher temporal resolution (~18 s). In addition, this method is insensitive to motion-induced susceptibility changes using the fat signal as the internal

reference.

Temperature sensitive MRI contrast agents

In comparison to the PRFS method, temperature mapping using the temperature-sensitive contrast agents offers about ten times greater sensitivity and possibility of obtaining absolute temperature measurements, although it suffers major disadvantages such as low signal intensity and requirement of contrast agent injection. Temperature measurements using paramagnetic chemical exchange saturation transfer (PARACEST) methods are based on the temperature modulation of the signal intensity or chemical shift of paramagnetic contrast agents (18). The chemical exchange rate (k_a) dependence on temperature follows Arrhenius equation {Eq. [1]}. Experimental results showed that a linear relationship exists between chemical shift (δ) and temperature over a small range (20–50 ℃) (76). That is,

$$\delta = \alpha T + \beta \qquad [6]$$

where α is the temperature coefficient and β is a constant which may depend on other physical parameters such as pH. Experimentally, ^{1}H signal from the temperature-sensing contrast agents can be directly observed using selective excitation because of the larger chemical shift separation (>200 ppm) relative to that of the bulk water signal. Alternatively, temperature measurement can also be achieved by saturating the ^{1}H signals in the PARACEST agent and then measuring the attenuated bulk water ^{1}H signal, similar to the MT technique used for endogenous contrast agents. By substituting the measured chemical shift into Eq. [6], absolute temperature in the ROI can be obtained.

Commonly used contrast agents are Lanthanide complexes, such as complexes of Pr^{3+}, Yb^{3+}, T^{3+}, Dy^{3+}, and Tm^{3+}. Among them, Tm^{3+} complexes are the most favorable ones. In particular, $TmDOTP^{5-}$ was used for *in vivo* temperature measurements at 4.7 T for both ^{1}H and ^{31}P nuclei over a temperature range of 25 to 32 ℃ (76). The measured temperature sensitivity was found to be 0.89 and 2.18 ppm/℃ for ^{1}H and ^{31}P chemical shifts in $TmDOTP^{5-}$, respectively. The compound is stable over a temperature range of 4 to 50 ℃. However, $TmDOTP^{5-}$ is sensitive to pH and Ca^{2+} in the tissue, causing temperature measurements inaccurate in the presence of these two interfering sources. To alleviate this problem, improved temperature-sensing lanthanide contrast agents were developed. The typical

one is $TmDOTA^-$, which is insensitive to pH and Ca^{2+} interference and safe for *in vivo* applications while retaining the high temperature sensitivity (77).

The toxicity of $TmDOTA^-$ is believed to be close to that of the $GdDOTA^-$ because of the similarity in molecular structure between the two compounds (77). For animal experiments, a dose of 1–2 mmoL/kg is normally used (78).

Another improved Tm^{3+} Lanthanide temperature sensing agent, $TmDOTMA^-$ was developed to afford narrower linewidth than that of $TmDOTA^-$ in addition to insensitivity to pH, Ca^{2+}, agent concentration, and other ions and macromolecules. The accuracy of temperature measurements achieved using $TmDOTMA^-$ in phantom and animals are 0.1 and 0.3 ℃, respectively. The $TmDOTMA^-$ concentration used for *in vivo* experiments should be about 1 mmol/kg (79). Combined improved MR spectroscopy imaging methods with $TmDOTMA^-$, *in vivo* temperature distribution in rat brain has been reported (*Figure 4*) (80).

Conclusions

As discussed above, MRI provides multiple temperature dependent parameters for thermal imaging, such as signal intensity, T1, T2, diffusion coefficient, magnetization transfer, PRFS (including phase imaging and spectroscopy) as well as frequency shift of temperature sensitive contrast agents. Although the issue with motion has been explored and new strategies have been proposed in several publications using a respiration triggered sequence (81,82), applying navigator echoes (83), or both (84), the results are still not ideal for patients with irregular breath and under situation when tumor tissues undergo irreversible shape transformation (for example, denature of protein after heating). Due to the fact that absolute temperature mapping techniques, including both spectroscopic imaging using metabolites as a reference and phase imaging using fat as a reference, are immune to susceptibility effects and are not dependent on phase differences, they are intrinsically more reliable than relative temperature measurement by phase mapping methods. With the development of new MR sequences, the low temporal and spatial resolution could be overcome and these methods may be preferred for future MR-guided thermal ablation systems. However, as of today, the most popular MR thermal imaging method applied in tumor thermal ablation surgery is still PRFS based phase mapping technique, which only provides relative temperature change and is prone to motion artifacts.
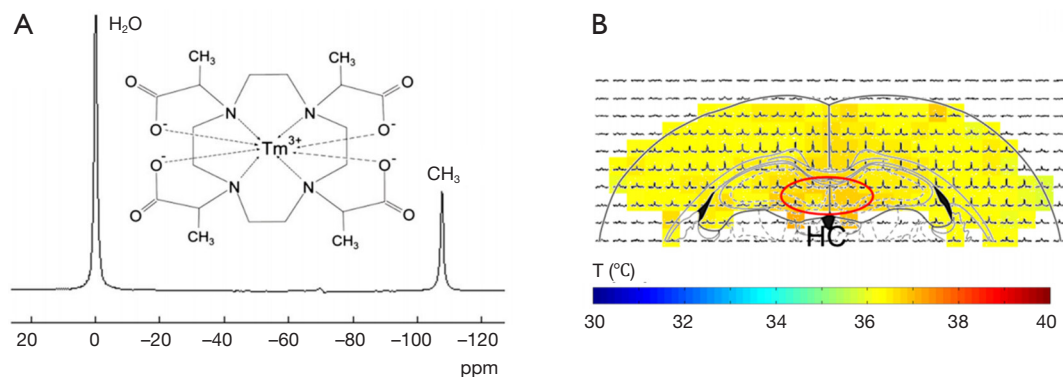
Figure 4 *In vivo* temperature distribution in rat brain measured by three-dimensional chemical shift imaging (3D CSI) with thulium 1,4,7,10-tetramethyl-1,4,7,10-tetraazacyclododecane-1,4,7,10-tetraacetate (TmDOTMA⁻) (80). (A) Chemical structure of TmDOTMA– and its proton MR spectrum. (B) Example from a 3D CSI slice in rat brain (–2.8 mm from the bregma). The temperature distribution was calculated to be 36.5±0.2 ℃. A temperature gradient of 0.3 ℃ across the cortex was observed. Moreover, significantly higher temperatures (0.5 ℃ compared with the cortex) was found in the hippocampus (HC, red oval).

Acknowledgements

Footnote

References

1. Hübner F, Bazrafshan B, Roland J, Kickhefel A, Vogl TJ. The influence of Nd:YAG laser irradiation on Fluoroptic(R) temperature measurement: an experimental evaluation. Lasers Med Sci 2013;28:487-96.

2. Manns F, Milne PJ, Gonzalez-Cirre X, Denham DB, Parel JM, Robinson DS. In situ temperature measurements with thermocouple probes during laser interstitial thermotherapy (LITT): quantification and correction of a measurement artifact. Lasers Surg Med 1998;23:94-103.

3. van der Zee J, Peer-Valstar JN, Rietveld PJ, de Graaf-Strukowska L, van Rhoon GC. Practical limitations of interstitial thermometry during deep hyperthermia. Int J Radiat Oncol Biol Phys 1998;40:1205-12.

4. Wust P, Gellermann J, Harder C, Tilly W, Rau B, Dinges S, Schlag P, Budach V, Felix R. Rationale for using invasive thermometry for regional hyperthermia of pelvic tumors. Int J Radiat Oncol Biol Phys 1998;41:1129-37.

5. Denis de Senneville B, Quesson B, Moonen CT. Magnetic resonance temperature imaging. Int J Hyperthermia

2005;21:515-31.

6. Quesson B, de Zwart JA, Moonen CT. Magnetic resonance temperature imaging for guidance of thermotherapy. J Magn Reson Imaging 2000;12:525-33.

7. Rieke V, Butts Pauly K. MR thermometry. J Magn Reson Imaging 2008;27:376-90.

8. Wust P, Cho CH, Hildebrandt B, Gellermann J. Thermal monitoring: invasive, minimal-invasive and non-invasive approaches. Int J Hyperthermia 2006;22:255-62.

9. Gellermann J, Wlodarczyk W, Feussner A, Fahling H, Nadobny J, Hildebrandt B, Felix R, Wust P. Methods and potentials of magnetic resonance imaging for monitoring radiofrequency hyperthermia in a hybrid system. Int J Hyperthermia 2005;21:497-513.

10. Parker DL, Smith V, Sheldon P, Crooks LE, Fussell L. Temperature distribution measurements in two-dimensional NMR imaging. Med Phys 1983;10:321-5.

11. Le Bihan D, Delannoy J, Levin RL. Temperature mapping with MR imaging of molecular diffusion: application to hyperthermia. Radiology 1989;171:853-7.

12. Chen J, Daniel BL, Pauly KB. Investigation of proton density for measuring tissue temperature. J Magn Reson Imaging 2006;23:430-4.

13. De Poorter J, De Wagter C, De Deene Y, Thomsen C, Stahlberg F, Achten E. Noninvasive MRI thermometry with the proton resonance frequency (PRF) method: in vivo results in human muscle. Magn Reson Med 1995;33:74-81.

14. Yuan J, Mei CS, Panych LP, McDannold NJ, Madore B. Towards fast and accurate temperature mapping with

proton resonance frequency-based MR thermometry. Quant Imaging Med Surg 2012;2:21-32.

15. Kuroda K, Mulkern RV, Oshio K, Panych LP, Nakai T, Moriya T, Okuda S, Hynynen K, Jolesz FA. Temperature mapping using the water proton chemical shift: self-referenced method with echo-planar spectroscopic imaging. Magn Reson Med 2000;43:220-5.

16. Kuroda K, Suzuki Y, Ishihara Y, Okamoto K, Suzuki Y. Temperature mapping using water proton chemical shift obtained with 3D-MRSI: feasibility in vivo. Magn Reson Med 1996;35:20-9.

17. Graham SJ, Bronskill MJ, Henkelman RM. Time and temperature dependence of MR parameters during thermal coagulation of ex vivo rabbit muscle. Magn Reson Med 1998;39:198-203.

18. Zuo CS, Metz KR, Sun Y, Sherry AD. NMR temperature measurements using a paramagnetic lanthanide complex. J Magn Reson 1998;133:53-60.

19. Lüdemann L, Wlodarczyk W, Nadobny J, Weihrauch M, Gellermann J, Wust P. Non-invasive magnetic resonance thermography during regional hyperthermia. Int J Hyperthermia 2010;26:273-82.

20. Craciunescu OI, Stauffer PR, Soher BJ, Wyatt CR, Arabe O, Maccarini P, Das SK, Cheng KS, Wong TZ, Jones EL, Dewhirst MW, Vujaskovic Z, MacFall JR. Accuracy of real time noninvasive temperature measurements using magnetic resonance thermal imaging in patients treated for high grade extremity soft tissue sarcomas. Med Phys 2009;36:4848-58.

21. Boss A, Graf H, Muller-Bierl B, Clasen S, Schmidt D, Pereira PL, Schick F. Magnetic susceptibility effects on the accuracy of MR temperature monitoring by the proton resonance frequency method. J Magn Reson Imaging 2005;22:813-20.

22. De Poorter J. Noninvasive MRI thermometry with the proton resonance frequency method: study of susceptibility effects. Magn Reson Med 1995;34:359-67.

23. Peters RD, Hinks RS, Henkelman RM. Heat-source orientation and geometry dependence in proton-resonance frequency shift magnetic resonance thermometry. Magn Reson Med 1999;41:909-18.

24. Kuroda K. Non-invasive MR thermography using the water proton chemical shift. Int J Hyperthermia 2005;21:547-60.

25. Kuroda K, Oshio K, Chung AH, Hynynen K, Jolesz FA. Temperature mapping using the water proton chemical shift: a chemical shift selective phase mapping method. Magn Reson Med 1997;38:845-51.

26. Bohris C, Schreiber WG, Jenne J, Simiantonakis I, Rastert R, Zabel HJ, Huber P, Bader R, Brix G. Quantitative MR temperature monitoring of high-intensity focused ultrasound therapy. Magn Reson Imaging 1999;17:603-10.

27. Chen L, Wansapura JP, Heit G, Butts K. Study of laser ablation in the in vivo rabbit brain with MR thermometry. J Magn Reson Imaging 2002;16:147-52.

28. Dragonu I, de Oliveira PL, Laurent C, Mougenot C, Grenier N, Moonen CT, Quesson B. Non-invasive determination of tissue thermal parameters from high intensity focused ultrasound treatment monitored by volumetric MRI thermometry. NMR Biomed 2009;22:843-51.

29. Nielsen OS, Horsman M, Overgaard J. A future for hyperthermia in cancer treatment? Eur J Cancer 2001;37:1587-9.

30. Napoli A, Anzidei M, Ciolina F, Marotta E, Cavallo Marincola B, Brachetti G, Di Mare L, Cartocci G, Boni F, Noce V, Bertaccini L, Catalano C. MR-Guided High-Intensity Focused Ultrasound: Current Status of an Emerging Technology. Cardiovasc Intervent Radiol 2013;36:1190-203.

31. Habash RW, Bansal R, Krewski D, Alhafid HT. Thermal therapy, Part III: ablation techniques. Crit Rev Biomed Eng 2007;35:37-121.

32. Brown SD, Vansonnenberg E, Morrison PR, Diller L, Shamberger RC. CT-guided radiofrequency ablation of pediatric Wilms tumor in a solitary kidney. Pediatr Radiol 2005;35:923-8.

33. Skjoldbye B, Burcharth F, Christensen JK, Moesgaard FA, Struckmann JR, Nolsoe CP. Ultrasound-guided radiofrequency ablation of malignant liver tumors. Ugeskr Laeger 2002;164:4646-50.

34. Brace CL. Radiofrequency and microwave ablation of the liver, lung, kidney, and bone: what are the differences? Curr Probl Diagn Radiol 2009;38:135-43.

35. Dupuy DE. Microwave ablation compared with radiofrequency ablation in lung tissue-is microwave not just for popcorn anymore? Radiology 2009;251:617-8.

36. Leonardi MA, Lumenta CB. Stereotactic guided laser-induced interstitial thermotherapy (SLITT) in gliomas with intraoperative morphologic monitoring in an open MR: clinical expierence. Minim Invasive Neurosurg 2002;45:201-7.

37. Reimer P, Bremer C, Horch C, Morgenroth C, Allkemper T, Schuierer G. MR-monitored LITT as a palliative concept in patients with high grade gliomas: preliminary clinical experience. J Magn Reson Imaging 1998;8:240-4.

38. Schwarzmaier HJ, Eickmeyer F, von Tempelhoff W, Fiedler VU, Niehoff H, Ulrich SD, Yang Q, Ulrich F. MR-guided laser-induced interstitial thermotherapy of recurrent glioblastoma multiforme: preliminary results in 16 patients. Eur J Radiol 2006;59:208-15.

39. Rieke V, Instrella R, Rosenberg J, Grissom W, Werner B, Martin E, Pauly KB. Comparison of temperature processing methods for monitoring focused ultrasound ablation in the brain. J Magn Reson Imaging 2013;38:1462-71.

40. Coakley FV, Foster BR, Farsad K, Hung AY, Wilder KJ, Amling CL, Caughey AB. Pelvic applications of MR-guided high intensity focused ultrasound. Abdom Imaging 2013;38:1120-9.

41. Pauly KB, Diederich CJ, Rieke V, Bouley D, Chen J, Nau WH, Ross AB, Kinsey AM, Sommer G. Magnetic resonance-guided high-intensity ultrasound ablation of the prostate. Top Magn Reson Imaging 2006;17:195-207.

42. Hokland SL, Pedersen M, Salomir R, Quesson B, Stodkilde-Jorgensen H, Moonen CT. MRI-guided focused ultrasound: methodology and applications. IEEE Trans Med Imaging 2006;25:723-31.

43. Vogl TJ, Mack MG, Straub R, Eichler K, Roggan A, Zangos S, Woitaschek D, Bottger M. Magnetic resonance (MR)-guided percutaneous laser-induced interstitial thermotherapy (LITT) for malignant liver tumors. Surg Technol Int 2002;10:89-98.

44. Burov AK. High-intensity ultrasonic vibrations for action on animal and human malignant tumors. Dokl Akad Nauk SSSR 1956;106:239-41.

45. Fry FJ. Precision high intensity focusing ultrasonic machines for surgery. Am J Phys Med 1958;37:152-6.

46. Hynynen K. MRI-guided focused ultrasound treatments. Ultrasonics 2010;50:221-9.

47. Hynynen K, Pomeroy O, Smith DN, Huber PE, McDannold NJ, Kettenbach J, Baum J, Singer S, Jolesz FA. MR imaging-guided focused ultrasound surgery of fibroadenomas in the breast: a feasibility study. Radiology 2001;219:176-85.

48. Mougenot P, Pinguet F, Fabbro M, Culine S, Poujol S, Astre C, Bressolle F. Population pharmacokinetics of melphalan, infused over a 24-hour period, in patients with advanced malignancies. Cancer Chemother Pharmacol 2004;53:503-12.

49. Palussière J, Salomir R, Le Bail B, Fawaz R, Quesson B, Grenier N, Moonen CT. Feasibility of MR-guided focused ultrasound with real-time temperature mapping and continuous sonication for ablation of VX2 carcinoma in rabbit thigh. Magn Reson Med 2003;49:89-98.

50. Salomir R, Palussiere J, Vimeux FC, de Zwart JA, Quesson B, Gauchet M, Lelong P, Pergrale J, Grenier N, Moonen CT. Local hyperthermia with MR-guided focused ultrasound: spiral trajectory of the focal point optimized for temperature uniformity in the target region. J Magn Reson Imaging 2000;12:571-83.

51. Machtinger R, Inbar Y, Cohen-Eylon S, Admon D, Alagem-Mizrachi A, Rabinovici J. MR-guided focus ultrasound (MRgFUS) for symptomatic uterine fibroids: predictors of treatment success. Hum Reprod 2012;27:3425-31.

52. Ringold S. FDA approves ultrasound fibroid therapy. JAMA 2004;292:2826.

53. Bettag M, Ulrich F, Schober R, Furst G, Langen KJ, Sabel M, Kiwit JC. Stereotactic laser therapy in cerebral gliomas. Acta Neurochir Suppl (Wien) 1991;52:81-3.

54. Schwabe B, Kahn T, Harth T, Ulrich F, Schwarzmaier HJ. Laser-induced thermal lesions in the human brain: short- and long-term appearance on MRI. J Comput Assist Tomogr 1997;21:818-25.

55. Schwarzmaier HJ, Yaroslavsky IV, Yaroslavsky AN, Fiedler V, Ulrich F, Kahn T. Treatment planning for MRI-guided laser-induced interstitial thermotherapy of brain tumors--the role of blood perfusion. J Magn Reson Imaging 1998;8:121-7.

56. Schwarzmaier HJ, Eickmeyer F, von Tempelhoff W, Fiedler VU, Niehoff H, Ulrich SD, Ulrich F. MR-guided laser irradiation of recurrent glioblastomas. J Magn Reson Imaging 2005;22:799-803.

57. Oto A, Sethi I, Karczmar G, McNichols R, Ivancevic MK, Stadler WM, Watson S, Eggener S. MR imaging-guided focal laser ablation for prostate cancer: phase I trial. Radiology 2013;267:932-40.

58. Tovar-Spinoza Z, Choi H. MRI-guided laser interstitial thermal therapy for the treatment of low-grade gliomas in children: a case-series review, description of the current technologies and perspectives. Childs Nerv Syst 2016;32:1947-56.

59. McDannold N. Quantitative MRI-based temperature mapping based on the proton resonant frequency shift: review of validation studies. Int J Hyperthermia 2005;21:533-46.

60. Ishihara Y, Calderon A, Watanabe H, Okamoto K, Suzuki Y, Kuroda K, Suzuki Y. A precise and fast temperature mapping using water proton chemical shift. Magn Reson Med 1995;34:814-23.

61. Sapareto SA, Dewey WC. Thermal dose determination in

cancer therapy. Int J Radiat Oncol Biol Phys 1984;10:787-800.

62. Roizin-Towle L, Pirro JP. The response of human and rodent cells to hyperthermia. Int J Radiat Oncol Biol Phys 1991;20:751-6.

63. Parker DL. Applications of NMR imaging in hyperthermia: an evaluation of the potential for localized tissue heating and noninvasive temperature monitoring. IEEE Trans Biomed Eng 1984;31:161-7.

64. Nelson TR, Tung SM. Temperature dependence of proton relaxation times in vitro. Magn Reson Imaging 1987;5:189-99.

65. Simpson JH, Carr HY. Diffusion and nuclear spin relaxation in water. Phys Rev 1958;111:1201-2.

66. Abragam A. The principles of the nuclear magnetism. New York: Oxford University Press 1983: 599.

67. Rimal V, Stepankova H, Stepanek J. Analysis of NMR spectra in case of temperature dependent chemical exchange between two unequally populated sites. Concept Magn Reson 2011;38A:117-27.

68. Wolff SD, Balaban RS. Magnetization transfer contrast (MTC) and tissue water proton relaxation in vivo. Magn Reson Med 1989;10:135-44.

69. Young IR, Hand JW, Oatridge A, Prior MV. Modeling and observation of temperature changes in vivo using MRI. Magn Reson Med 1994;32:358-69.

70. Soher BJ, Wyatt C, Reeder SB, MacFall JR. Noninvasive temperature mapping with MRI using chemical shift water-fat separation. Magn Reson Med 2010;63:1238-46.

71. Cady EB, D'Souza PC, Penrice J, Lorek A. The estimation of local brain temperature by in vivo 1H magnetic resonance spectroscopy. Magn Reson Med 1995;33:862-7.

72. Corbett RJ, Laptook AR, Tollefsbol G, Kim B. Validation of a noninvasive method to measure brain temperature in vivo using 1H NMR spectroscopy. J Neurochem 1995;64:1224-30.

73. Zhu M, Bashir A, Ackerman JJ, Yablonskiy DA. Improved calibration technique for in vivo proton MRS thermometry for brain temperature measurement. Magn Reson Med 2008;60:536-41.

74. Martin M, Labouesse J, Canioni P, Merle M. N-acetyl-L-aspartate and acetate 1H NMR signal overlapping under mild acidic pH conditions. Magn Reson Med 1993;29:692-4.

75. Covaciu L, Weis J, Bengtsson C, Allers M, Lunderquist A, Ahlstrom H, Rubertsson S. Brain temperature in volunteers subjected to intranasal cooling. Intensive Care Med 2011;37:1277-84.

76. Zuo CS, Bowers JL, Metz KR, Nosaka T, Sherry AD, Clouse ME. TmDOTP5-: a substance for NMR temperature measurements in vivo. Magn Reson Med 1996;36:955-9.

77. Zuo CS, Mahmood A, Sherry AD. TmDOTA-: a sensitive probe for MR thermometry in vivo. J Magn Reson 2001;151:101-6.

78. Hekmatyar SK, Poptani H, Babsky A, Leeper DB, Bansal N. Non-invasive magnetic resonance thermometry using thulium-1,4,7,10-tetraazacyclododecane-1,4,7,10-tetraacetate (TmDOTA(-)). Int J Hyperthermia 2002;18:165-79.

79. Hekmatyar SK, Hopewell P, Pakin SK, Babsky A, Bansal N. Noninvasive MR thermometry using paramagnetic lanthanide complexes of 1,4,7,10-tetraazacyclodoecane-alpha,alpha',alpha'',alpha'''-tetramethyl-1,4,7,10-tetraacetic acid (DOTMA4-). Magn Reson Med 2005;53:294-303.

80. Coman D, de Graaf RA, Rothman DL, Hyder F. In vivo three-dimensional molecular imaging with Biosensor Imaging of Redundant Deviation in Shifts (BIRDS) at high spatiotemporal resolution. NMR Biomed 2013;26:1589-95.

81. Lepetit-Coiffé M, Quesson B, Seror O, Dumont E, Le Bail B, Moonen CT, Trillaud H. Real-time monitoring of radiofrequency ablation of rabbit liver by respiratory-gated quantitative temperature MRI. J Magn Reson Imaging 2006;24:152-9.

82. Morikawa S, Inubushi T, Kurumi Y, Naka S, Sato K, Demura K, Tani T, Haque HA. Feasibility of respiratory triggering for MR-guided microwave ablation of liver tumors under general anesthesia. Cardiovasc Intervent Radiol 2004;27:370-3.

83. de Zwart JA, Vimeux FC, Palussiere J, Salomir R, Quesson B, Delalande C, Moonen CT. On-line correction and visualization of motion during MRI-controlled hyperthermia. Magn Reson Med 2001;45:128-37.

84. Vigen KK, Daniel BL, Pauly JM, Butts K. Triggered, navigated, multi-baseline method for proton resonance frequency temperature mapping with respiratory motion. Magn Reson Med 2003;50:1003-10.